Develop a Supercapacitor Real Time Model for PHIL Simulation

Baochen Li

A thesis

submitted in partial fulfillment of the

requirements for the degree of

Master of Science

University of Washington

2019

Committee:

Daniel Schwartz

Venkat Subramanian

Program Authorized to Offer Degree:

Chemical Engineering

University of Washington

Abstract

Develop a Supercapacitor Real Time Model for PHIL Simulation

Baochen Li

Chair of the Supervisory Committee:
Daniel Schwartz
Department of Chemical Engineering

Energy generation devices, like solar cells and fuel cells, can rarely meet all of the dynamic behavior of variable loads, which results in load performance limitations. Therefore, energy storage devices, like batteries and supercapacitors, are introduced into the system to ensure quality power is provided under a wide range of dynamic load conditions. Hardware-in-the-loop (HIL) and power-hardware-in-the-loop (PHIL) real time simulations are among the most reliable methods for ensuring generation and storage can meet load demands in real time, because it is executed physically rather than as a purely computational exercise. My research is focused on developing supercapacitor implementations for HIL and PHIL. For supercapacitors, equivalent circuit model can adequately represent the dynamic behavior, but this kind of model can be difficult to ascribe to physical meanings, which is significant for designing and scaling-up a commercial supercapacitor device. An expression-based equivalent circuit model is used to solve this problem. Parameters in the model can be linked with configuration parameters of an actual

device. A Simulink model is then loaded in our OPAL-RT real time simulator, which together with power amplifier and programmable load, allow power hardware-in-the-loop real time supercapacitor discharge simulations. The PHIL results are shown to be limited by the ± 1 V and ±3 A hardware noise. To achieve higher voltages than allowed by a single cell, multiple cells get connected in series and parallel to achieve enough voltage and power. We show how a Simulink supercapacitor module can be built with passive balancing to achieve good module performance while limiting excessive potential on individual cells.

TABLE OF CONTENTS

LIST OF FIGURES

LIST OF TABLES

Chapter 1. Introduction

1.1 Real Time Simulation and PHIL Simulation

Real time simulation refers to a computer model of a physical system that can execute at a rate fast enough to capture the critical dynamics of a system, as it is operating. For batteries and super capacitors, this execution time is usually tens of milliseconds. Computer languages like LabVIEW, VisSim and Simulink allow quick creation of such real-time simulations and connect to industrial displays and Programmable Logic Controllers for process control or digital and analog I/O cards. Several software platforms are common for real-time simulators, such as Simulink, eFPGAsim and eDRIVEsim for power electronic simulation and eMEGAsim, HYPERSIM and RTDS for power grid real-time simulation (RTS) [1]. Simulink is a graphical programming environment for modeling and simulating and analyzing multidomain dynamic systems developed by MathWorks [2], which is well accepted in Opal-RT, a real time hardware-in-the-loop simulator (HIL). Power Hardware-in-the-loop (PHIL) simulation refers to the inclusion of real-world power hardware in the simulation loop. Creating models of some power components to run in real time enables the mixing of simulated and physical power hardware components in a PHIL simulation. PHIL is significant in developing integrated systems, reducing costs and shortening design cycle. Simulink is used to build the models, and here we focus on the energy generating and storage components like fuel cells, batteries, and supercapacitors, where the model is used to drive a power amplifier that emulate and deliver the actual power to meet load demand. In this way, different simulated generation configurations can be matched to a real variable load, such as an electric vehicle drive train, a power grid component, or programmable load to assess the system performance. In Simulink, power system models can be built based on math and electronic elements blocks given by Simulink library or through governing equations

of physical system via Matlab function and solver, using a block that solves equations by readable commands.

1.2 Energy storage devices

Matching the electrical demand from a load to the generated supply of electricity can be challenging, and that is where energy storage comes into play. The variable nature of the energy supply from renewable sources, like solar and wind, means at different times there can be a mismatch between supply and demand. Likewise, the inability of slow-response energy devices, like solid oxide fuel cell, means a fast-dynamic load cannot be followed [3]. Therefore, energy storage devices are introduced into the system to compensate for this difference and provide high quality uninterrupted power. The most common energy storage devices are batteries and supercapacitors, both of which are built based on the electrochemical conversion between electrical and chemical energy [4]. Rechargeable electrochemical energy storage devices transfer electrical energy to chemical energy during charging and converts chemical energy to generate electrical energy at the period of discharging through a reversible electrochemical reaction. A basic electrochemical storage device consists of two electrodes separated by a porous separator filled by electrolyte. Fig 1.1 shows the Ragone plot of some typical electrochemical energy conversion and storage devices, where EDLC denotes an “electrochemical double layer capacitor”.

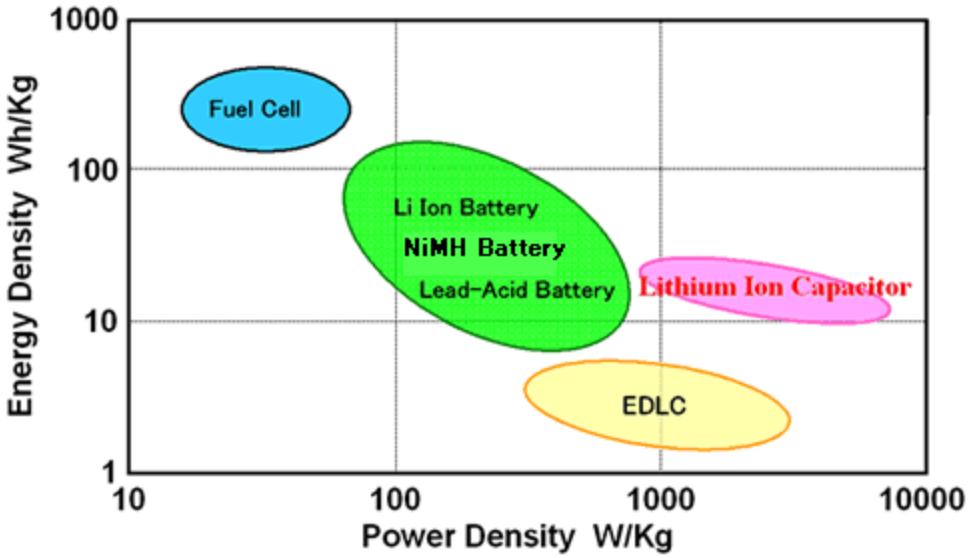

Fig. 1.1 Ragone plot [5] of electrochemical devices with characteristics of their power and energy densities.

1.2.1 Supercapacitors

Supercapacitors (SC), also known as ultracapacitors, store energy in an electrochemical double-layer (e.g., ELDC in Figure 1.1) or through electrochemical reactions (e.g. Li Ion Capacitor in Figure 1.1) on large surface porous electrodes. They have much higher energy densities than traditional dielectric capacitors. The first commercially successful supercapacitor cell was manufactured by Nippon Electric Company in 1971 [6]. Since then, supercapacitors have become attractive as energy storage devices and are under fast development. As shown in Figure 1.1, compared with batteries or fuel cells, ECDL and Li-ion capacitors have the advantages of high-power density, meaning fast charge and discharge rate, as well as a long cyclic life and wide range operating temperature, but they also exhibit poor total energy density and high self-discharge rate [4,7,8]. Due to these disadvantages, supercapacitors are usually connected in

parallel with other energy supply devices to form an uninterrupted power system, ensuring qualified power supplement. Unlike batteries, there is no nominal voltage over a large portion of the discharge curve for supercapacitors, which means they cannot hold a nearly fixed voltage for a duration of time. To achieve steady voltage from supercapacitors, DC to DC converters are introduced to the hybrid system for DC applications.

1.2.2 Batteries

Batteries can be categorized into two types, primary batteries and secondary batteries [4]. Primary batteries cannot be charged due to the irreversible electrochemical reactions taking place in it. Zinc-carbon batteries, alkaline batteries, and lithium-metal batteries all can be manufactured as primary batteries. They come in a charged form, consume the limited chemical energy inside, and generate electrical energy. Therefore, high performance primary batteries normally have specialized application such as medical devices or military uses, where there is a small predictable load (e.g. hearing aid, pace maker) or single use devices (e.g., bombs, torpedoes). Low cost consumer batteries have traditionally been primary batteries, but they are going out of favor owing to their disposal issues tied to heavy metals and corrosive electrolytes, resulting in decrease of primary battery manufactures for cells such as zinc-carbon batteries [9].

Secondary batteries allow repeated energy storage and conversion cycles. Lead-acid batteries, flow batteries, lithium-ion batteries, nickel-cadmium batteries all can be manufactured as secondary batteries, and they widely used in high performance applications that require untethered electrical devices (power tools, cell phones, etc.) and especially electric vehicles [4]. They store energy via displacement reactions and/or intercalation of ions into electrodes [10]. Displacement reactions are the reactions which more active ions replace less active ion in the

solid phase to electrolyte. On the other hand, ions are inserted into the lattice of electrodes in intercalation reactions. With reaction going on, ions are directed through separator to the other electrode and electrons migrate via external circuit generating current. As shown in Figure 1.1, secondary batteries generally exhibit higher energy density than supercapacitors due to electrodes full volume participating in storage, rather than just the interfacial regions [3]. But this volumetric energy storage is also responsible for the lower power available for high rate charge and discharge, as also shown in Figure 1.1. After hundreds or thousands of charge and discharge cycles, battery electrodes will degrade, in part, caused by expansion of electrode lattice in intercalation mechanism batteries. Therefore, secondary batteries tend to have a shorter cyclic life than supercapacitors.

1.3 Type of Supercapacitors

Supercapacitors can be categorized as symmetric or asymmetric based on whether there is a difference in electrode materials [7]. Symmetric supercapacitors are fabricated with the same material for both cathode and anode. For asymmetric supercapacitors, two electrodes are made with different materials, such as two different carbon material or one carbon electrode together with one metal oxide electrode. Hybrid supercapacitors are asymmetric, developed for high power and energy density [11]. Their two electrodes are the combination of one capacitive material and one Faradaic capacitive material. Here, capacitive materials refer to the materials that exhibit capacitance either by electric double layer physical attraction of ions or by fast surface redox reactions. Faradaic capacity is the capacitance generated through slow redox reaction, which is commonly used in batteries. In other words, hybrid supercapacitor is a combination of supercapacitor and battery. A lithium ion capacitor is a typical hybrid supercapacitor. Supercapacitors are also categorized into electrical double layer capacitors and

pseudocapacitors based on these same energy storage mechanism (via double layer or Faradaic electrochemical reaction processes).

1.3.1 Electrical Double Layer Capacitors

Electrical double layer capacitors (EDLCs) are the most common commercial supercapacitors. A single commercial EDLC cell will typically have a performance of two to three volts and hundreds to thousands of Faradays of capacitance. Electrical double layer refers to Stern layer where some ions adhere to the electrodes along with the diffuse layer in which ion distribution is a function of distance from electrode surface. Considering the solvent action in electrode/electrolyte interface, physicochemical model such as the Bockris/Devanathan/Muller (BDM) approach can be built for EDLC [12].

When EDLC is charged, ions of electrolytes are transferred and absorbed on the surface of the electrode of opposite polarity, generating double layer capacitance. Voltage distribution across a charged ELDC and ions behavior during charging in a BDM model are shown in Fig.1.2. These ions are desorbed from electrode surface and diffuse back into electrolyte while EDLC is under discharge.

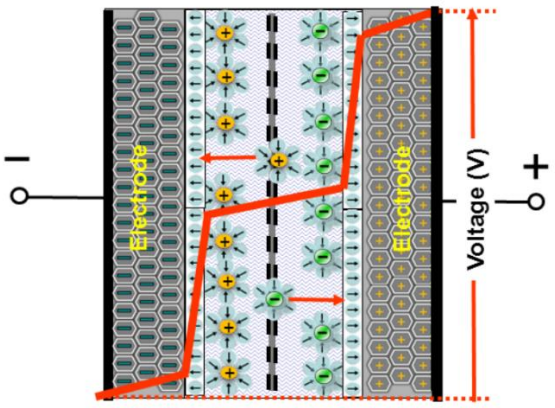

Fig.1.2 Voltage distribution across a charged EDLC. [13]

1.3.2 Pseudocapacitors

Pseudocapacitors are the supercapacitors that storage energy not only by electrostatic attraction but also with electrochemical Faradaic reactions. As a result, energy density of pseudocapacitors is higher than that of EDLCs and close to that of batteries. Pseudocapacitors were first discovered by Conway and Birss in 1975 [14,15]. Nowadays, research of pseudocapacitors is ongoing with material that can achieve high energy density and fast charge-discharge rate.

Underpotential deposition, redox reaction and intercalation are the three mechanisms for building pseudocapacitors. Underpotential deposition is a phenomena of a metal deposits at a potential less than Nernst potential for reduction [16], which only occurs at the formation of first deposition monolayer. Redox reaction is the reaction occurring with reduction and oxidation. Reduction indicates electrons are accepted and oxidation state goes lower, while oxidation is the opposite. Intercalation means that the cations in electrolyte are inserted into electrode lattice. With the existence of these mechanisms, pseudocapacitors can store more energy than pure electrostatic attraction in EDLCs. Metal oxides and conductive polymers are traditional electrodes in pseudocapacitors. In addition, a great load of research on graphene materials as pseudocapacitor electrodes are reported due to their good electrical conductivity and compatibility in recent decades. Both aqueous and organic based solution can be used as electrolyte in pseudocapacitors. Limitations for aqueous electrolyte is the small operation voltage and poor cycle life. The standard potential difference of water electrolysis is 1.23 volts [17], which limits the voltage window for aqueous pseudocapacitors. Moreover, gases produced through the chemical reactions expand electrode structure leading to electrode degradation and hence reducing capacitance in each charge and discharge cycle. On the other hand, using organic

electrolyte can overcome the two main limitations caused by aqueous electrolyte but shrinks the available capacitance.

1.4 Supercapacitor Equivalent circuit models

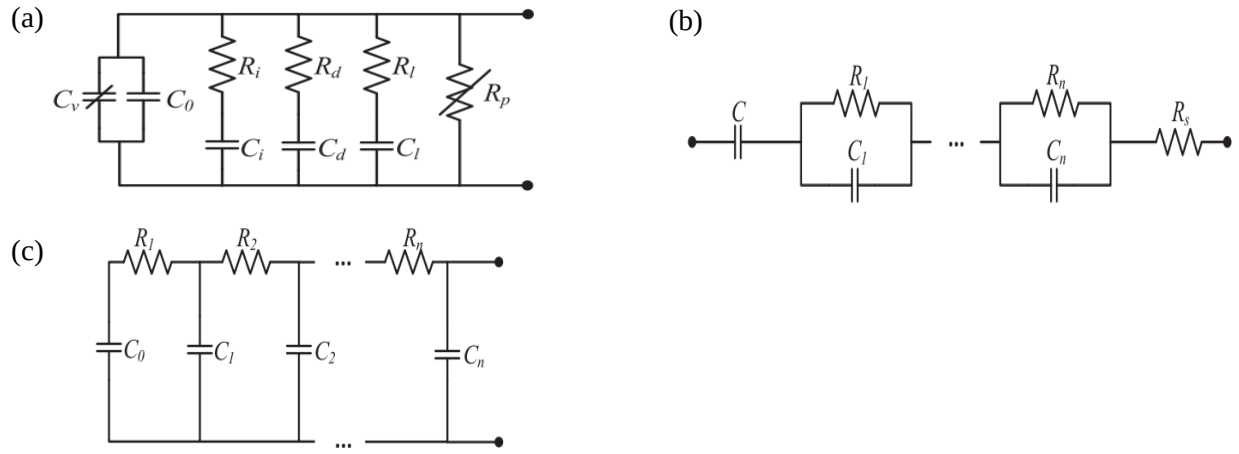

Fig.1.3 (a) to (c) existing different equivalent circuit models for SCs.

Equivalent circuit models are built based on circuit elements and relatively simple structure maintaining reasonable precision in terms of the dynamic behavior of a supercapacitor (SC). In industry, a SC equivalent circuit model has three parts, equivalent series resistance (ESR), equivalent parallel resistance (EPR), and capacitance [18]. Parameter values from this industry model is strongly dependent on SC state of charge. A three resistor-capacitor (RC) branch model, Figure 1.3(a), dynamic model, Figure 1.3(b), and ladder model Figure 1.3(c), are also commonly derived as a way to simulate SC behavior accurately with less dependence on state of charge. These models can capture the various dynamic SC behaviors seen at different response time constants, represented by separate RC elements. Figure 1.3(a) shows three RC time constants, usually ranging from a few seconds (immediate branch), a few minutes (delay branch), to dozens of minutes (long-term branch). The dynamic model, shown in Fig.1.3 (b), consists of a main capacitance, an internal resistance and several RC elements. It successfully describes SC

behavior in terms of electrochemical impedance spectrum (EIS). The ladder model, shown in Fig.1.3 (c), is derived to describe the charge spatial redistribution phenomena inside SCs [19]. Among them, the dynamic model has the best overall performance in terms of model complexity, precision, and robustness [20,21]. Therefore, SC dynamic model is used as the basic SC model for PHIL real time simulation in this research.

Chapter 2. Experimental Methods

2.1 Experimental Equipment and Software

Experiments: All equipment is available at the Washington Clean Energy Testbeds. We used the Opal RT real time simulator, programmable power (AMETEK, MX30), a resistive heater load, a programmable load (AMETEK), impedance analysis workstation (VersaSTAT 4000), and a commercial supercapacitor (Maxwell 2.7V 1500F). This equipment was operated in a standard mode.

Software: Simulink from MathWorks was used to develop dynamic models that ran on the Opal RT simulator, using RT-Lab on the Opal RT.

2.2 EDLC Equivalent Circuit Model parameters estimation

Even though the dynamic model can fit the impedance result perfectly, the parameters in it can lack physical meaning. Hence, a method of relating EDLC dynamic model parameters with configuration parameters is required. De Levie [22,23] described the impedance of porous electrodes via distributed element model, also known as transmission line illustrated as Fig.2.1. Governing equations for such electrical circuit model are listed in Eq. (1).

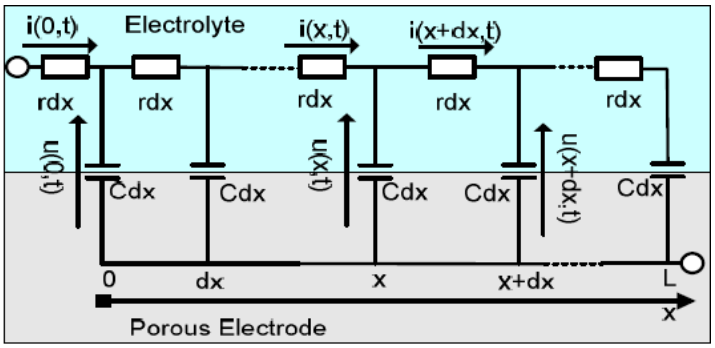

Fig.2.1 Transmission line schematic of interface between electrolyte and electrode [23].

(1)

$$\frac{\partial u(x,t)}{\partial x} = -\frac{R}{L} \cdot i(x,t); \quad \frac{\partial i(x,t)}{\partial x} = -\frac{C}{L}\frac{\partial u(x,t)}{\partial t},$$

Where, u(x,t) is the local dynamic voltage; x is direction through porous electrode; R is pore total resistance, mΩ; L is thickness of the electrode, μm; i(x,t) is the local dynamic current; C is pore total capacitance, F.

Eq. (2) is the resulting porous electrode impedance which can work properly for the electrodes in EDLCs (usually activated carbons). Therefore, as shown in Fig.2.2, the impedance of EDLCs can be presented by adding a contact resistance (R_c [mΩ]) to De Levie's impedance.

$$Z = \frac{\tau \cdot \coth\sqrt{j\omega\tau}}{C \cdot \sqrt{j\omega\tau}} \tag{2}$$

Where, τ is the pore time constant equal to the product of total pore resistance R and total pore capacitance C, s; j is the unit imaginary number, square root of -1; ω is angular frequency, rad/s.

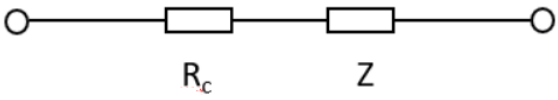

Fig.2.2 Schematic for impedance of EDLC based on De Levie's expression.

According to the definition of Fourier complex coefficient value, hyperbolic cotangent function can be approximately expressed as Eq. (3) derived from the series of a 2π-periodic function f(x) = e^{ax} [24]. Eq. (4) can be derived by replacing Eq. (3) in Eq. (2). In Eq. (4), the first term is the impedance for a capacitor and the second term is the impedance for a sum of CR elements. Therefore, the equivalent circuit model for EDLCs can be expressed as Fig.1.3 (b) with fixed circuit elements regrading to the three parameters R_c, τ, and C, as shown in Fig.2.3 [25].

$$\coth x = \frac{1}{x} + 2\sum_{n=1}^{\infty} \frac{x}{x^2+n^2\pi^2} \tag{3}$$

$$Z = \frac{\tau \cdot coth\sqrt{j\omega\tau}}{C\cdot\sqrt{j\omega\tau}} = \frac{1}{j\omega C} + \sum_{n=1}^{\infty} \frac{\frac{2\tau}{n^2\pi^2 C}}{j\omega\frac{\tau}{n^2\pi^2}+1} \tag{4}$$

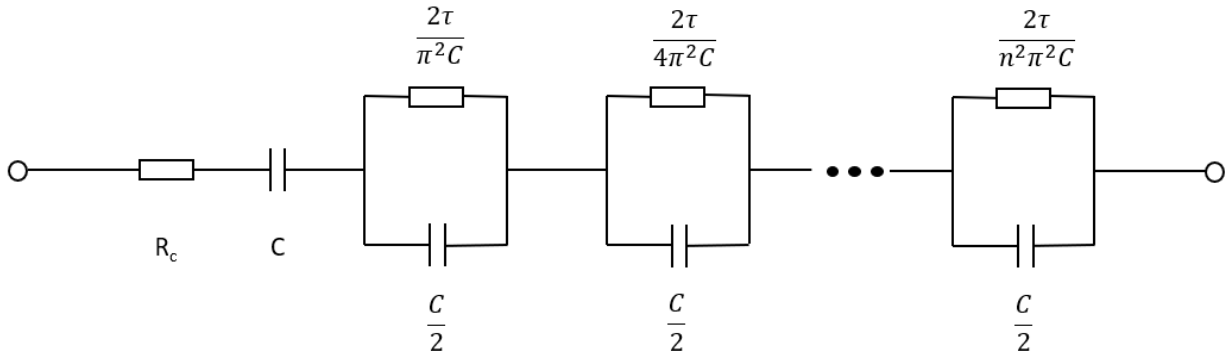

Fig.2.3 Equivalent circuit model gained by De Levie's expression.

Then, an impedance analysis for Maxwell 2.7 V 1500 F single EDLC was run by Versa STAT workstation from 10 Hz to 0.1 Hz. In order to estimate parameters, least square of the combination of real part and imaginary part on the Nyquist plot was used as the criteria for a good fitting to impedance result. Fitting results could be interpreted based on configuration parameters, such as electrode thickness, electrode conductivity, electrode porosity, electrolyte conductivity, and separator thickness. After parameters were estimated, an EDLC equivalent circuit model was built in Simulink. To examine the accuracy of equivalent circuit model, a step changed constant current discharge test profile was run to compare the voltage difference between Maxwell EDLC single cell and the model. After that, the model was built in Opal-RT and prepared for PHIL real time simulation of the Maxwell supercapacitor.

2.3 EDLC single cell PHIL simulation

Power Hardware in the loop (PHIL) simulation is set up as shown in Fig.2.4. Equivalent circuit model is load in Opal-RT machine, which sends the voltage value signal to power amplifier, controlling the power amplifier so it behaves like a real supercapacitor. Output voltage provided by power amplifier is connected to power a programmable load, generating a current passing through the circuit. Passing current is measured by current clamps and sent to the model in Opal-RT to determine output voltage for the next loop. In Fig.2.4, black lines stand for the wire in circuit; blue lines represent the direction of signal flow used as feedback in the model run by the Opal-RT.

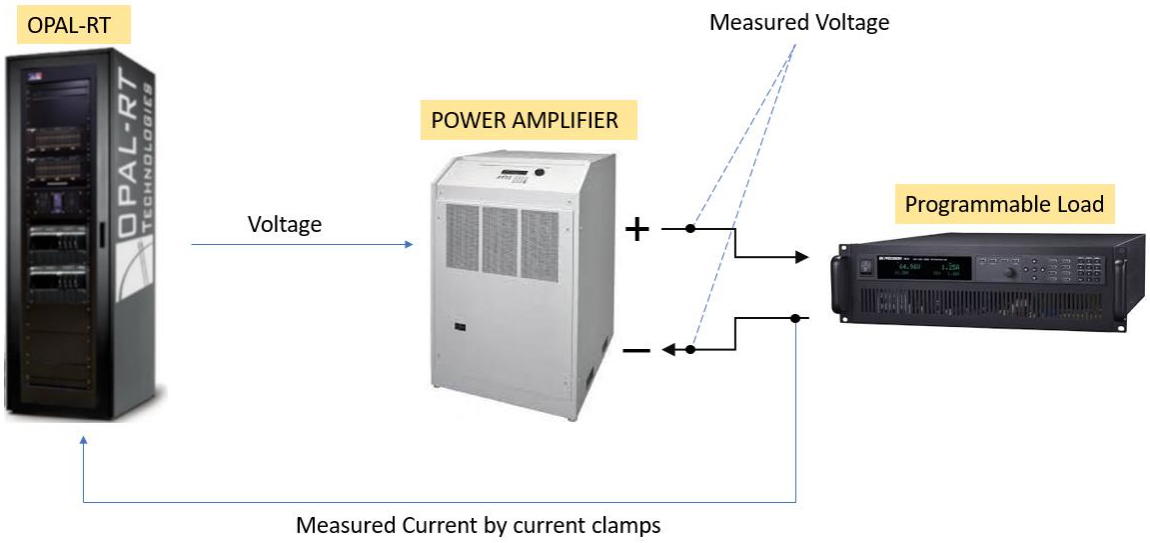

Fig.2.4 PHIL simulation hardware setup schematic.

Blocks built in Opal-RT is shown in Fig.2.5. The SC model simulation is run in the subsystem with current as input and voltage as output sending to power amplifier for PHIL simulation. Voltage is measured from power amplifier and current is measured through programmable load via current clamps. Since Opal-RT machine is manufactured for AC application, it has three voltage signal and three current signal outputs. Nevertheless, in this research, Opal-RT is applied for a DC application. Three phase voltages and currents signal are decomposed and only one

phase signal is needed. Moreover, the input current is read from Opal-RT AnalogIn block (signal from current clamps) to match hardware setup. Measured voltage and current data are recorded in Matlab from Opal-RT ports.

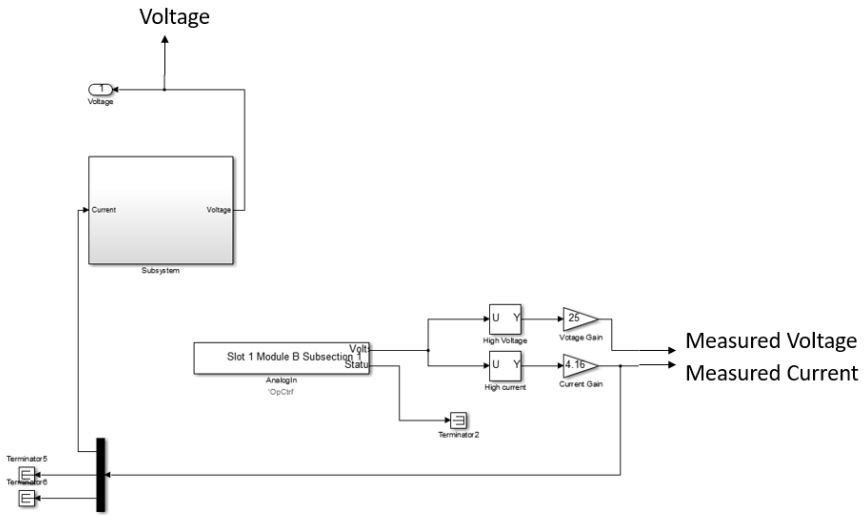

Fig.2.5 Schematic of blocks built in Opal-RT.

2.4 EDLC module with passive balancing

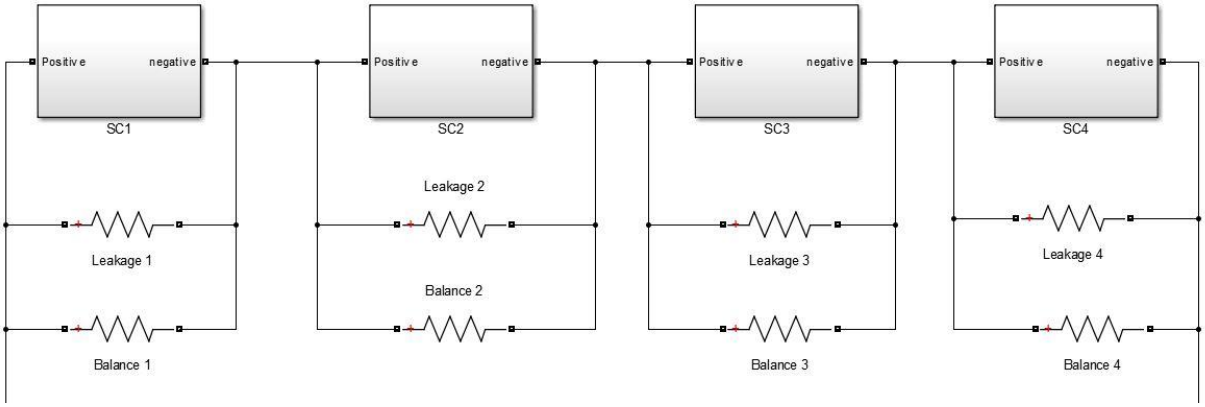

Fig.2.6 EDLC pack with passive balancing in Simulink.

The typical commercial EDLC has a maximum voltage of two to three Volts. Considering this low operation voltage and the required voltage of uninterrupted power systems, it is necessary to connect EDLC single cells in series, forming a pack, to achieve a suitable working voltage. All ELCD SC devices have some natural variance in capacitances, internal resistances, and leakage current, no matter how well manufactured, so the voltage distribution on EDLCs in such a serial connection will not be uniform [26]. Therefore, it is possible that individual EDLC in the pack may exceed the rated voltage while charging, causing degradation after certain usage cycles. To prevent from this case, voltage crossed EDLC cells should be equalized by adding balancing systems. Balancing systems can be divided into passive balancing and active balancing. Passive balancing utilizes equal resistors connecting in parallel with EDLC to force voltage between each cell the same by dissipating extra energy from charging. Metal-oxide semiconductor field-effect transistor is introduced into active balancing system to regulate voltage distribution among individual cells. Compared with passive balancing, active balancing has the advantages of saving energy but it is hard for design and also expensive. In this research, passive balancing strategy is introduced into the pack to guarantee voltage across different EDLCs below their nominal voltage, as shown in Fig.2.6.

Chapter 3. Results and Discussion

3.1 EDLC single cell simulation

Fig.3.1 compares the measured Maxwell 2.7 V 1500 F EDLC impedance Nyquist diagram with the result of simulation based on De Levie's expression. The red plot in the figure indicating De Levie's expression can overlap with EIS result of Maxwell 1500 F with least square fit. But the impedance of two RC elements dynamic model with variables derived from De Levie expression has a significant difference from EIS experimental data. This difference is generated by the approximation made in hyperbolic cotangent function in De Levie expression, Eq. (3). The definition of Fourier complex coefficient is the average coefficient value across the period. Therefore, it is an optimal value instead of a coefficient by analytical solution. Moreover, only two RC elements are used in model, instead of many RC elements, because it is inefficient to build a single EDLC with that many elements. These two reasons are why impedance diagram of the equivalent circuit model with expression parameter values has such a big difference with experiment result.

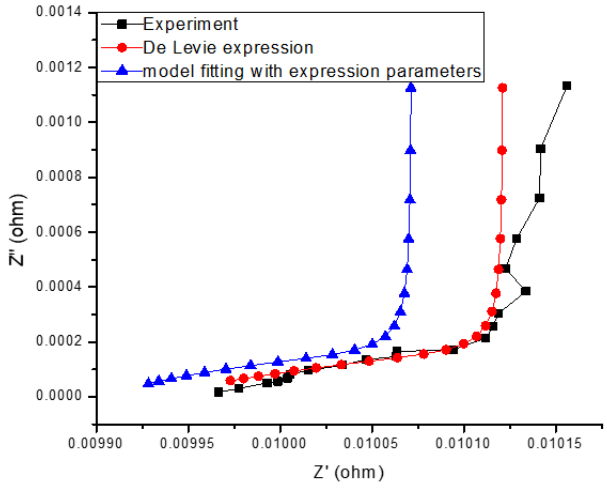

Fig.3.1 Nyquist plot of EIS and De Levie expression fitting results.

Hence, value of parameters in Eq. (4) was gained through calculating the least squares between experiment data and the equivalent circuit model. Considering accuracy and complicity of the model, two RC elements are used in dynamic model. As shown in Fig.3.2, it is well matched with EIS result. Parameter value from this result can represent the dynamic behavior of Maxwell EDLCs and be further linked with physical configurations.

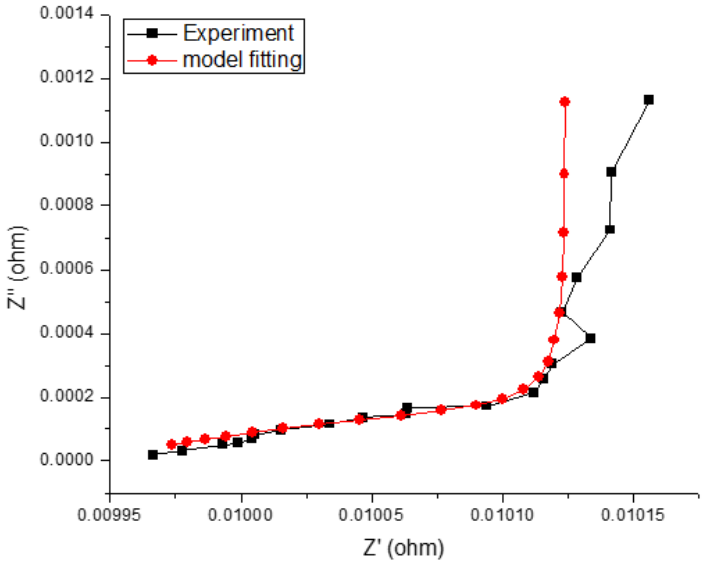

Fig.3.2 Nyquist plot of equivalent circuit model and EIS.

To test the accuracy of the dynamic model and parameter value, a step changing constant DC discharge profile was tested between Maxwell EDLC and the model. Due to the current limitation from the workstation, high constant current discharge cannot be tested through Maxwell EDLC. Instead, a high current EDLC discharge profile is run with programmable load. Unlike batteries, EDLCs go through the same path while they are being charged and discharged [27] because activation overpotentials are not involved in EDLCs electrical storage mechanism. Therefore, EDLC equivalent circuit models can also be applied under the situation of being charged though only discharge current profile is tested. The dynamic model was built in

Simulink using parameter values from model fitting. In Fig.3.3, voltage response to the same current profile (a) for both EDLC model (black line in (b)) and Maxwell EDLC (red line in (b)) is compared. A difference in a magnitude of dozens of millivolts is observed at the moment when current had a step change, shown in (c). This difference can be explained by the limited sampling rate of programmable load which leads to a delay when voltage changes rapidly [25]. Overall, dynamic model can perfectly simulate the charge and discharge performance of a Maxwell EDLC, within the sampling constraints of the programmable load.

(a)

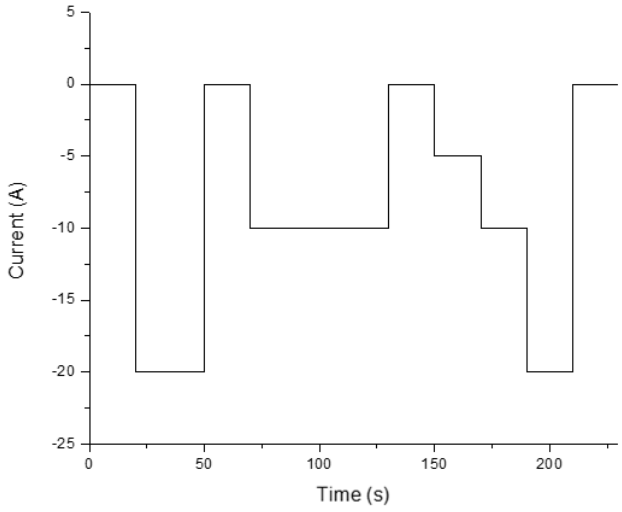

(b)

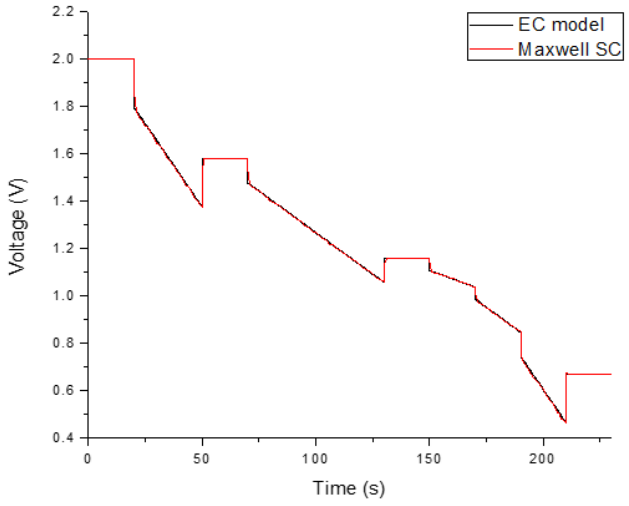

(c)

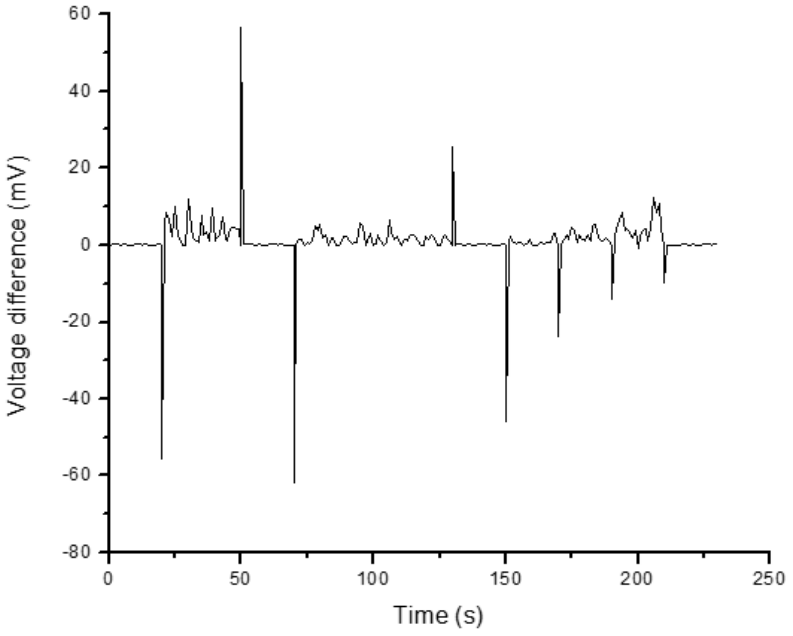

Fig.3.3 (a) Testing current profile for both Equivalent circuit model and Maxwell supercapacitor; (b) voltage response to current profile in (a); (c) voltage difference between experiment and simulation.

According to the datasheets provided by Maxwell, there is a linear relationship between capacitance and length of this series of EDLCs [28]. As mentioned before, parameters in dynamic model are estimated from De Levie's expression to link with configuration values. Therefore, a unique EDLC can be designed to meet specific application requirements by changing configuration variables. Typically, an EDLC consists of symmetric electrodes, electrolyte, separator and current collector. Activated carbon used as electrodes; 1 mol/L $TEMABF_4$ solved in acetonitrile as electrolyte; cellulose made commercialized TF4425 as separator; Aluminum with a thickness of 30 μm as current collector. Physical variables and corresponding values are listed in Table 3-1.

Table 3-1 Physical variables of Maxwell 2.7 V 1500 F EDLC [29-31].

	Electrodes		Electrolyte		Separator
L_e	50 μm	κ	50.2 mS/cm	L_s	25 μm
σ	0.727 mS/cm			κ_s	0.738 mS/cm
ε	0.6				
ρ	0.45 g/cm3				

In this table, L_e is electrode thickness; σ is electrode conductivity; ε is the porosity of the electrode; ρ is the density of electrode; κ is electrolyte conductivity; L_s is separator thickness; κ_s is the conductivity of 1 M $TEMABF_4$/acetonitrile in TF4425.

From pervious least square fitting of the model to the experimental Nyquist plot, the best fit parameters were C = 1425 F, R_i = 9.96 mΩ, τ = 0.926 s. These measured values can be related to physically meaningful variables via the following expressions.

$$C_p = \frac{C_v S L_e}{2};\ R_p = \frac{L_e}{\frac{\kappa'\sigma'}{\kappa'+\sigma'}S};\ R_s = \frac{L_s}{\kappa_s S};\ R_i = R_s + R_c\,, \tag{5}$$

Where, the product of C_p and R_p is τ; C_v is the capacitance density (F/cm^3); S is the cross-section area [32]; κ', σ' are efficient conductivities; R_c is the contact resistance.

Here, a capacitance density was used instead the formula of dielectric capacitance in [32]. This is because the electrolyte molecular behavior around the porous electrode is different from normal, making the dielectric constant of acetonitrile inequal to its bulk value. Therefore, the determining parameters for capacitance are lumped together in capacitance density. Electrode tortuosity was achieved from porosity by the means of Bruggeman correlation with a value of 0.5. Afterwards,

efficient conductivity was determined by the McMullin number. Specific capacitance density and cross-section area were found to be 54.8 F/g and 2.3 m^2, which were reasonable values compared to references [33-35]. Based on this analysis, EDLC materials and sizes could be adjusted to build a proper EDLC device for powering alternative loads, like hybrid electrical vehicles, grids, and data centers.

The Simulink model with measured and scalable parameters, was loaded in Opal-RT and PHIL real-time simulation was set up. Based on the power amplifier manual, the power amplifier was not able to operate at 2.7 V, so the initial voltage in the model was adjusted as 10 V. To match server rack operation current, one of the SC power applications we are interested in, the programmable load was set as resistance of 0.4 Ω or 0.8 Ω. PHIL simulation voltage and current response is shown in Fig.3.4 for a 1000 s total run. The circuit was closed at 100 s to allow current flow, and opened at 900 s, to stop current. Therefore, voltage was held at the first and last 100 seconds. The pike occurred every 100 seconds in current response was caused by the same cycle settings in programmable load. The trends of current and voltage change were correct but they were obscured by the ±1 V noise in the power amplifier. For example, in resistance step change experiment in Fig.3.4 (e) & (f), a blur of change could be detected.

(a)

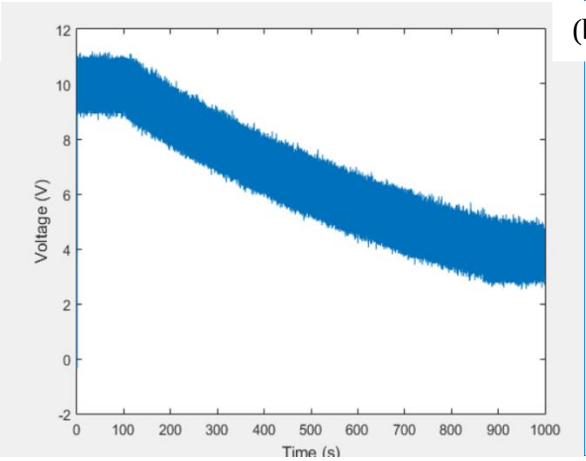

(b)

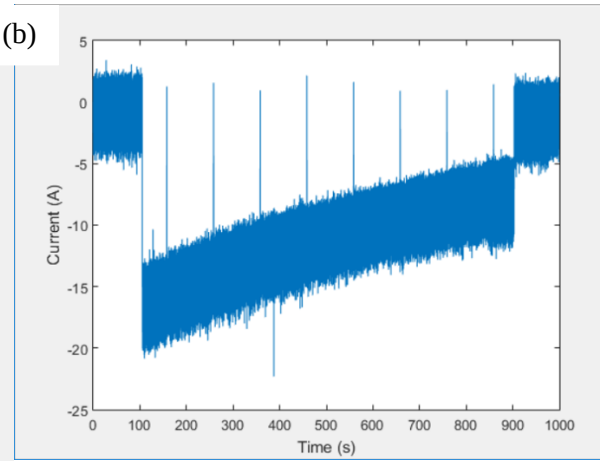

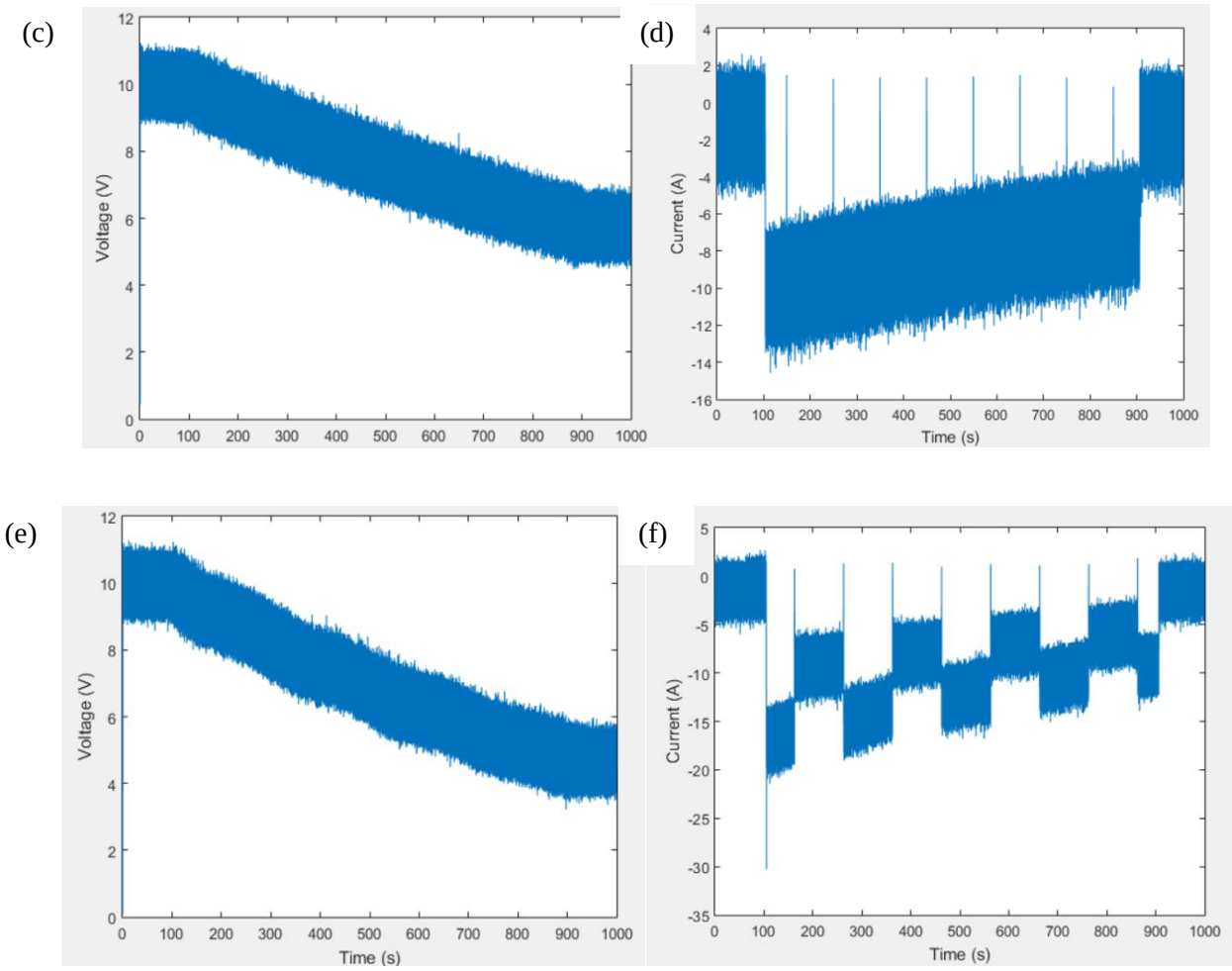

Fig.3.4 (a), (b) Voltage and current response of constant 0.4 Ω; (c), (d) Voltage and current response of constant 0.8 Ω; (e), (f) Voltage and current response of step-change 0.4 Ω and 0.8 Ω. alternation.

Voltage response had a fluctuation of ±1 V, while current response oscillated around ±3 A. Voltage data was read from power amplifier and current data was measured via current clamps, which means this noise in current was presumably caused by current clamps. Therefore, new methods are being developed to reduce the noise in current reading. Moreover, there was a non-linear voltage drop between power amplifier and programmable load in PHIL simulation shown in Table 3-2, which is caused by inner settings of the programmable load. This voltage drop is

small when the programmable load is set as a high resistance. Measured current was gained based on voltage between programmable load and setting resistance. Since the state of charge in the model was calculated by measured current, this drop made the PHIL simulated EDLC produce less energy than a real EDLC. But this voltage drop can be eliminated if the programmable load is replaced by a real load, like a heater or a server rack. Therefore, PHIL simulation is still helpful in designing power devices as well as identifying potential problems in power systems for specific applications.

Table 3-2 Voltage difference between power amplifier and programmable load.

Voltage (V)	100 s (power amplifier)	100 s (programmable load)	900 s (power amplifier)	900 s (programmable load)
0.4 Ω	10.00	8.13	3.97	3.19
0.8 Ω	10.00	9.00	5.86	5.23
0.4 Ω & 0.8 Ω step change	10.00	8.13 (0.4 Ω at 100 s)	4.78	3.87

3.2 EDLC module simulation

EDLC single cells are connected in series to achieve adequate supply voltage. However, EDLCs have some variation in key specifications even though they are manufactured under the same procedures. To ensure voltage across each cell is not exceeding the EDLC nominal voltage (2.7 V), balancing is used to redistribute voltage. Therefore, a small EDLC module model (10 V) was built based on Maxwell datasheet [36]. To build a module, leakage currents of each single cell should be considered beyond the parameters already mentioned in models. To represent this self-

leakage phenomenon, a leakage resistance was added in parallel with the EDLC model. Standard value of leakage resistance was nominal voltage divided by leakage current in [28]. Within a multi-cell module, the parameters used in the EDLC model, including Ri, C, τ, and leakage resistance, were allowed to vary by ±10 % around standard value for the individual EDLC cell. The solid line in Fig. 3.5 represents the calculated voltage distribution of a module without passive balancing. The second cell in the module is operating at an excessive voltage, which may lead to degradation of the whole module. Passive balancing was achieved by using resistors added in parallel again to ensure a balanced voltage. Balancing resistor have a value of approximate one tenth of standard leakage resistor [37]. Simulation result with passive balancing are shown as Fig. 3.5 with the dash line. Voltages from each cell are maintained below the nominal voltage when passive balancing is used, and all approach the same value. This EDLC module has a leakage current of 29 mA, which is similar to a real module [36].

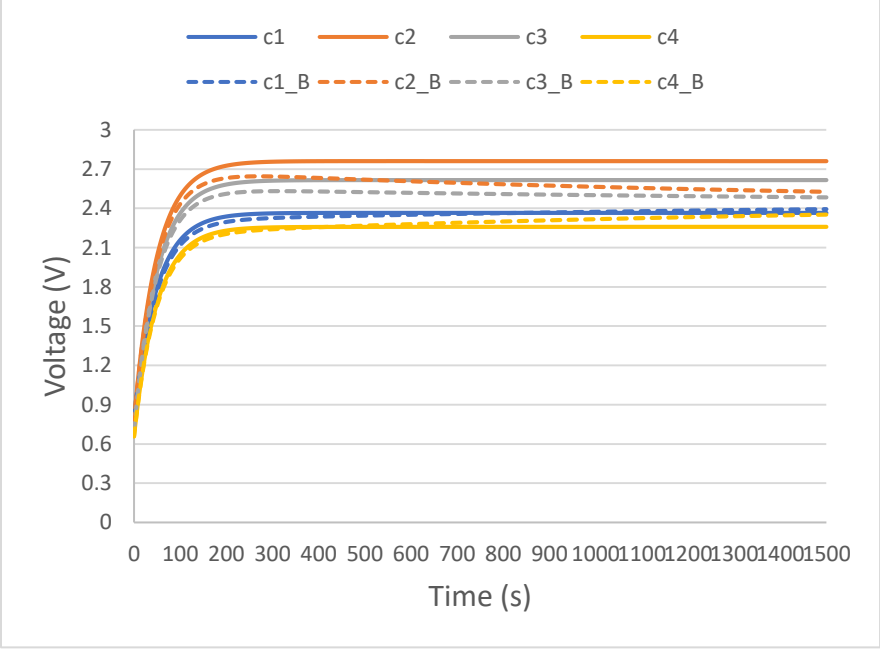

Fig.3.5 Voltage distribution during charging with/without passive balancing.

Chapter 4. Conclusion

In conclusion, an equivalent circuit EDLC model with parameters linked to physical configuration was built for PHIL simulation. Firstly, an EDLC model was built based on De Levie's expression for porous electrode. Due to the optimal coefficient value used in hyperbolic cotangent approximation, as well as limitation of adding RC elements, a difference existed between the expression and the model in impedance result. Therefore, the two RC dynamic model was developed to serve as the basis for parameter estimation via least square fitting. Discharge tests demonstrated that this model could represent the dynamic behavior of a Maxwell 2.7 V 1500 F EDLC. A relationship between estimated parameters and the properties of electrodes, electrolyte, separator was revealed to be within reasonable ranges for the physical device. By connecting measured parameters to cell properties, EDLC materials and sizes could be scaled to build a proper EDLC device for powering dynamic loads. The model was then applied in PHIL simulation. From the result, voltage response had a fluctuation of ±1 V but current response had a noise of ±3 A. New methods are being developed to collect accurate current data. The voltage drop observed among power amplifier and programmable load could be eliminated by replacing programmable load with actual loads. Finally, an EDLC module model was built with passive balancing, which may be tested by PHIL simulation in the future.

ACKNOWLEDGEMENTS

I want to express my sincere appreciation to my advisor Professor Daniel Schwartz for his guidance and encouragement, my group members Maitri Uppaluri, Yusong Liu, Erica Eggleton, Victor Hu, Yanbo Qi, and Linnette Teo for their helpful advice, and my parents for their invaluable support.

References

[1] Real-time simulation, https://en.wikipedia.org/wiki/Real-time_simulation

[2] Simulink, https://en.wikipedia.org/wiki/Simulink

[3] Venkataraman Anuradha, Pseudocapacitors for Energy Storage, 2015, Dissertations and Theses, Paper 2486.

[4] Haisheng Chen, Thang Ngoc Cong, Progress in electrical energy storage system: A critical review, Progress in Natural Science, 19, 2009: 291-312.

[5] Ragone Plot, https://en.wikipedia.org/wiki/Ragone_plot

[6] Immanuel Jiya, Nicoloy Gurusinghe. Electrical circuit modelling of double layer capacitors for power electronics and energy storage applications: a review. Electronics, 2018, 7, 268.

[7] Ander González, Eider Goikolea, Review on supercapacitors: Technologies and materials, Renewable and Sustainable Energy Reviews 58, 2016: 1189–1206.

[8] Nathalie Devillers, Samir Jemei, Review of characterization methods for supercapacitor modelling, J. Power Sources, 246, 2014: 596-608.

[9] A.M. Bernardes, D.C.R. Espinosa, Recycling of batteries: a review of current processes and technologies, J. Power Sources, 130, 2004: 291-298.

[10] Zhe Li, Jun Huang, A review of lithium deposition in lithium-ion and lithium metal secondary batteries, J. Power Sources, 254, 2014: 168-182.

[11] Guoping Wang, Lei Zhang, A review of electrode materials for electrochemical supercapaciors, Chem. Soc. Rev., 41, 2012: 797-828.

[12] J. O'M. Bockris, M. A. V Devanathan, and K. Mueller, On the structure of charged interfaces, Electrochemistry, 1965: 832-863.

[13] EDLC voltage distribution,

https://upload.wikimedia.org/wikipedia/commons/d/da/EDLC-Voltage_distribution.png

[14] B.E. Conway, V. Birss, J. Wojtowicz, The Role and Utilization of Pseudocapacitance for Energy Storage by Supercapacitors, Journal of Power Sources, 66, 1997:1-14.

[15] B. E. Conway, Transition from "Supercapacitor" to "Battery" Behavior in Electrochemical Energy Storage, J. Electrochem. Soc. 138, 1991 :1539-1548.

[16] Underpotential deposition, https://en.wikipedia.org/wiki/Underpotential_deposition

[17] Electrolysis of water, https://en.wikipedia.org/wiki/Electrolysis_of_water

[18] Equivalent circuit model, skeleton technologies white paper equivalent series resistance.

[19] F. Belhachem, S. Rael, A physical based model of power electric double-layer supercapacitors, IEEE industry applications conference, 2000: 3069-3076.

[20] Lei Zhang, Zhenpo Wang, A comparative study of equivalent circuit models of ultracapacitors for electric vehicles, Journal of Power Sources, 274, 2015: 899-906.

[21] Lei Zhang, Xiaosong Hu, A review of supercapacitor modeling, estimation, and applications: A control/management perspective, Renewable and Sustainable Energy Reviews, 81, 2018: 1868–1878.

[22] R. De Levie, Electrochemical Response of porous and rough electrodes, in: Advances in Electrochemistry and Electrochemical Engineering, 6, 329-397, 1967, Wiley Interscience, New York, London, Sydney.

[23] H. Brouji, J. Vinassa, Ultracapacitors self-discharge modelling using a physical description of porous electrode impedance. IEEE VPPC, September, 2008.

[24] Hyperbolic cotangent transformation, https://math.stackexchange.com/questions/845506/series-expansion-of-coth-x-using-the-fourier-transform

[25] S. Buller, Modeling the Dynamic Behavior of Supercapacitors Using Impedance Spectroscopy, Conference of the 2001 IEEE Industry Applications Conference.

[26] Tomislav Baric, Supercapacitors, cell balancing using resistors, UDK: 621.175.4, 2018: 15-22.

[27] Ultracapacitor discharge curve, https://www.tecategroup.com/ultracapacitors-supercapacitors/ultracapacitor-FAQ.php

[28] Maxwell ultracapacitor cells, https://www.maxwell.com/products/ultracapacitors/cells

[29] Mark Verbrugge, Ping Liu, Microstructural analysis and mathematical modeling of Electric Double-layer supercapacitors, J. Electrochemical Society, 152 (5), 2005: D79-D87.

[30] M. Harmas, Carbon for Energy storage derived from granulated white sugar by hydrothermal carbonization and subsequent zinc chloride activation, J. Electrochemical Society, 164 (9), 2017: A1866-A1872.

[31] K. Tonurist, A. Janes. Influence of mesoporous separator properties on the parameters of EDLC single cells, J. Electrochemical Society,156 (4), 2009: A334-A342.

[32] M. Kroupa, Modeling of Supercapacitors: Factors Influencing Performance. J. Electrochemical Society, 163 (10), 2016: A2475-A2487.

[33] R. Drummond, D. A. Howey, Low-order mathematical modelling of electric double layer supercapacitors using spectral methods, J. Power Sources, 277, 2015: 317-328.

[34] C. Portet, P.L. Taberna. High power density electrodes for carbon supercapacitor applications, Electrochimica Acta, 50, 2005: 4174-4181.

[35] W. Pell, Voltammetry at a de Levie brush electrode as a model for electrochemical supercapacitor behavior, Journal of Electroanalytical Chemistry, 500, 2001: 121–133.

[36] Maxwell supercapacitor module, https://www.maxwell.com/images/documents/240V_3_75F_ds_3001973_datasheet.pdf

[37] Yi cheng Zhang, Li Wei, Study of Supercapacitor in the Application of Power Electronics, J. WSEAS Transactions on Circuits and Systems, 6, 8, 2009: 508-517.